Surface Orientation in the Sheet of a Liquid Crystalline Poly(ester amide) Characterized by Reflection Infrared Spectroscopy

A. Kaito* and K. Nakayama

Research Institute for Polymers and Textiles, 1-1-4 Higashi, Tsukuba, Ibaraki 305, Japan

Received September 3, 1991; Revised Manuscript Received April 2, 1992

ABSTRACT: Polarized reflection infrared spectroscopy was applied to characterize the surface orientation of extrusion molded sheets of a liquid crystalline poly(ester amide) polymerized from 2-hydroxy-6-naphthoic acid, 4-aminophenol, and terephthalic acid. One of the spectroscopic methods studied in this work is specular reflection infrared spectroscopy, in which the absorption and refractive indices are calculated from the specular reflectance by using the Fresnel equation and the Kramers-Kronig relation. Another technique used for the analysis is polarized ATR spectroscopy, which gives the three-dimensional components of the absorption index. The polarized ATR spectrum is in excellent agreement with the spectrum obtained from the specular reflection measurement in the spectral region where only weak absorption bands exist. Intense absorption bands in the ATR spectrum are, however, influenced by the large refractive index dispersion. At a lower draw-down ratio, the surface orientation function is higher than the bulk orientation function obtained from the azimuthal intensity distribution of wide-angle X-ray diffraction. The bulk orientation function increases with increasing draw-down ratio, and the difference between the surface and bulk orientation functions is smaller at higher draw-down ratio.

Introduction

A surface of polymeric materials sometimes exhibits a unique structure that is different from the bulk. One of the most stimulating examples is a fabric of a liquid crystalline polymer that exhibits a skin-core structure with a highly oriented skin layer and less ordered core region.[1-5]

The structure of polymer surface has been extensively studied by means of attenuated total reflection (ATR)/Fourier-transform infrared (FTIR) spectroscopy. ATR/FTIR spectroscopy using polarized infrared radiation was successfully applied to characterize the molecular orientation at the surface of stretched polymer sheets.[6-10] The orientation profiles in the plaques of a thermotropic liquid crystalline polymer were obtained by the ATR/FTIR technique.[11] More recently the depth profile of surface crystallinity of polyethylene film was studied by ATR/FTIR spectroscopy.[12]

Flournoy and Schaeffers reported a theoretical formulation for polarized ATR spectroscopy of anisotropic films,[13] in which the reflectivities for polarized radiation were related to the three components of absorption index. Although the theory for ATR spectroscopy is established, it is a matter for due consideration that the intensity of the ATR spectrum is sensitive to the contact area between the sample and the ATR crystal. In order to obtain a dichroic ATR spectrum, the sample should be rotated and might be remounted. If the sample is remounted, however, the contact area is not reproduced. In order to solve the problem, Sung and co-workers[6,7,11] designed a rotatable ATR sample holder and a square ATR crystal, which allow us to rotate the sample without remounting it.

On the other hand, specular reflection spectroscopy has been extensively studied in the visible-ultraviolet region[14-21] as well as in the infrared-far-infrared region,[22-24] in order to measure the spectrum of single crystals. Recently we have reported that the specular reflection measurements with polarized radiation are useful for analyzing the surface orientation of polymer sheets.[25,26] The polarized electronic spectra of oriented aromatic polymers were obtained from the specular reflectance in the visible-ultraviolet region by using the Kramers-Kronig relation and the Fresnel equation. The orientation function at the surface was evaluated from the dichroic ratios of the electronic absorption bands.[25,26]

In this work, polarized ATR/FTIR spectroscopy and polarized specular reflection FTIR spectroscopy are used to characterize the surface orientation of extrusion molded sheets of a thermotropic liquid crystalline polymer. We compare the polarized FTIR spectrum obtained from the specular reflection measurements with the polarized ATR/FTIR spectrum and discuss the validity of the reflection FTIR spectroscopy as a probe for the surface structure.

Experimental Section

Sample Preparation. The sample studied in this work is a poly(ester amide) polymerized from 2-hydroxy-6-naphthoic acid, 4-aminophenol, and terephthalic acid. The polymer exhibits a crystal-mesophase transition at 283 °C. Pellets of the poly(ester amide) was obtained from Polyplastic Co., Ltd. The pellets were dried at 90 °C for 12 h and 150 °C for 3 h. Oriented sheets were extrusion molded by using a twin-screw extruder equipped with a coat-hanger die. The width of the die orifice was 150 mm, and the die gap was adjusted at 2 mm. The die temperature was controlled at 290 ± 2 °C. The extruded sheets were stretched in the molten state after leaving the die exit and were slowly cooled to ambient temperature. The mass output in the extrusion molding was kept constant throughout the experiments. The draw-down ratio was controlled by changing the take-up velocity. In this work, the sheets with draw-down ratios of 4.07 and 13.8 are picked out for the measurements.

Measurements. Reflection FTIR spectra were measured on a Perkin-Elmer Model 1800 FTIR spectrometer equipped with a liquid nitrogen cooled MCT detector. The 500-1000 scans of 4-cm^{-1} resolution were averaged to obtain a sufficient signal-to-noise ratio. The polarized reflection spectra were obtained by placing two wire-grid polarizers at the entrance and the exit of the reflection apparatus.

The specular reflection FTIR spectra were measured with a 10° angle of incidence by using a specular reflection accessory produced by Perkin-Elmer Co., Ltd. The reference spectrum was obtained with an aluminum plane mirror. In order to remove surface impurities, the surface of samples was washed by ligroin and acetone prior to the measurements. The geometry for the specular reflection measurements is shown in Figure 1, where the X and Y axes are parallel to the extrusion direction (ED) and the transverse direction (TD), respectively, and the Z axis is normal to the sheet plane. The sample sheet was mounted on

0024-9297/92/2225-4882$03.00/0

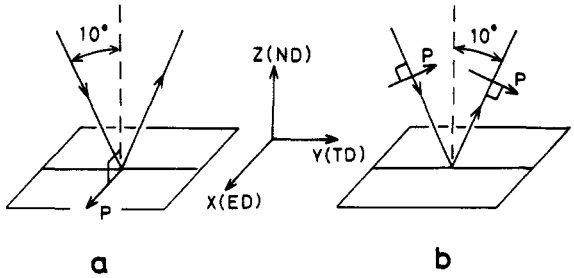

Figure 1. Coordinate system for specular reflection measurements. The polarization direction is shown by *P*: (a) polarization direction is normal to the plane of incidence; (b) polarization direction lies in the plane of incidence.

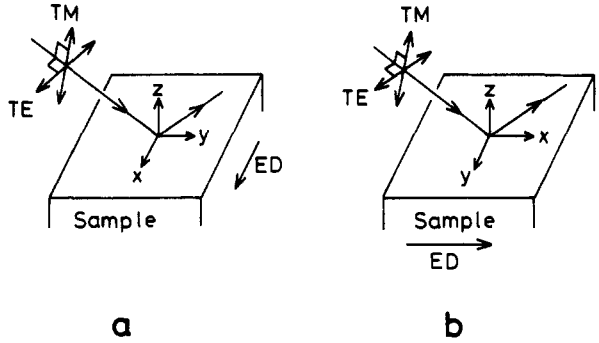

Figure 2. Coordinate system for ATR measurements. The polarization directions for transverse electric wave and transverse magnetic wave are indicated by TE and TM, respectively: (a) extrusion direction is set normal to the plane of incidence; (b) transverse direction is set normal to the plane of incidence.

the sample holder with the extrusion direction (*X* axis) perpendicular to the plane of incidence. The dichroism in reflectance was obtained by changing the polarization direction. The polarization direction is parallel to the *X* axis (extrusion direction) in Figure 1a. The polarization direction lies in the plane of incidence (*Y*–*Z* plane) and perpendicular to the extrusion direction in Figure 1b.

The ATR accessory used in this work (Harrick Scientific Corp.) is composed of a germanium ATR crystal (25 mm × 25 mm × 2 mm) and a rotatable sample holder. The apparatus was first designed by Sung and co-workers.[6,7] The four edges of the square crystal are cut at a 45° angle from the top and bottom planes. ATR spectra were measured at a 45° angle of incidence. The entrance and exit facets of the ATR attachment were masked in order to remove the stray radiation.

The coordinate system for ATR measurements is shown in Figure 2. The electric field vector of the transverse magnetic wave (TM) lies in the plane of incidence, while that for the transverse electric wave (TE) is perpendicular to the plane of incidence. The sample sheet is mounted on the ATR apparatus with the extrusion direction perpendicular to the plane of incidence in Figure 2a, while the transverse direction is set perpendicular to the plane of incidence in Figure 2b. Four components of polarized ATR spectrum were obtained by rotating the sample and the polarizer.

The crystal orientation function in the bulk was determined from the azimuthal intensity distribution of wide-angle X-ray diffraction (WAXD). Ni-filtered Cu Kα radiation generated by a Geigerflex XGC-20 (Rigaku Denki Co., Ltd.) was used as an incident X-ray beam. The WAXD intensity was measured by using a scintillation counter and a pulse height analyzer.

Analysis

Determination of Optical Constants from Specular Reflectance. The incident light beam is reflected only at the front surface of sample sheets in the region of strong absorption, while there is a contribution to the observed reflectance from multiple reflections at both surfaces of the sample in the transparent region.[15,25] In the case of transparent sheets, the reflectance at the front surface can be obtained with the correction of multiple reflection.[15] The strong absorption bands of the poly(ester amide) are fairly overlapping in the wavenumber region 550–1900 cm^{-1}, and the transmittance of the sample sheet is lower than 13% in this spectral region. In this work, the observed reflectance was corrected for the multiple reflection, but the reflectance was modified only slightly by the correction.

The reflection data were analyzed by use of the Fresnel equation for the normal incidence. The reflectance at normal incidence was evaluated by scaling the observed reflectance measured at a 10° angle of incidence:

$$R_p(0°) = C_p R_p(10°) \tag{1}$$

$$R_s(0°) = C_s R_s(10°) \tag{2}$$

where $R_p(\chi)$ and $R_s(\chi)$ are reflectances at an angle of incidence, χ, for the incident radiation polarized parallel and perpendicular, respectively, to the plane of incidence. The reflectances, R_s and R_p, are measured with the geometries shown in parts a and b of Figure 1, respectively. With increasing angle of incidence in the small-angle range, R_p decreases, but R_s increases. The values of scaling constants C_p and C_s are calculated to be 1.037 and 0.964, respectively for $n = 1.55$ and $k = 0.5$. These values are only weakly dependent on the angle of incidence in the small-angle range and are not so sensitive to refractive and absorption indices.[25]

Reflection from the absorption medium is accompanied by a phase shift, ϕ. According to the Fresnel equation at normal incidence, the refractive index, n, and the absorption index, k, are expressed in terms of R and ϕ as follows:

$$n = (1 - R)/(1 + R - 2R^{1/2}\cos\phi) \tag{3}$$

$$k = -2R^{1/2}\sin\phi/(1 + R - 2R^{1/2}\cos\phi) \tag{4}$$

The phase shift, $\phi(\nu_0)$, at wavenumber ν_0 can be calculated from the dispersion of reflectance by use of the Kramers–Kronig relation.

$$\phi(\nu_0) = \frac{1}{\pi}\int_0^\infty \left|\frac{\nu + \nu_0}{\nu - \nu_0}\right| \frac{d \ln [R(\nu)]^{1/2}}{d\nu} d\nu \tag{5}$$

As the reflectance can be measured in the limited spectral range, the contribution to $\phi(\nu_0)$ from the reflectance outside the measurable region is not explicitly known. The major contributions to $\phi(\nu_0)$, however, come from the reflectance in the neighborhood of ν_0, because the function $\ln|(\nu + \nu_0)/(\nu - \nu_0)|$ is strongly peaked at $\nu = \nu_0$. In this work, the integration in eq 5 was carried out in the wavenumber range 550–1900 cm^{-1}, and the contribution from the reflectance outside the measured region was evaluated by the equation proposed by Roessler:[18,19]

$$\phi(\nu_0) = \phi_a(\nu_0) + \phi_1(\nu_0) + \phi_b(\nu_0) \tag{6}$$

$$\phi_1(\nu_0) = \frac{1}{\pi}\int_a^b \left|\frac{\nu + \nu_0}{\nu - \nu_0}\right| \frac{d \ln [R(\nu)]^{1/2}}{d\nu} d\nu \tag{7}$$

$$\phi_a(\nu_0) = A \ln\left|\frac{a + \nu_0}{a - \nu_0}\right| \tag{8}$$

$$\phi_b(\nu_0) = B \ln\left|\frac{b + \nu_0}{b - \nu_0}\right| \tag{9}$$

$\phi_1(\nu_0)$ is the contribution from the region between a and b, in which the reflection spectrum is measured. $\phi_a(\nu_0)$ is the contribution from the wavenumber region below a, and $\phi_b(\nu_0)$ is the contribution from the region above b.

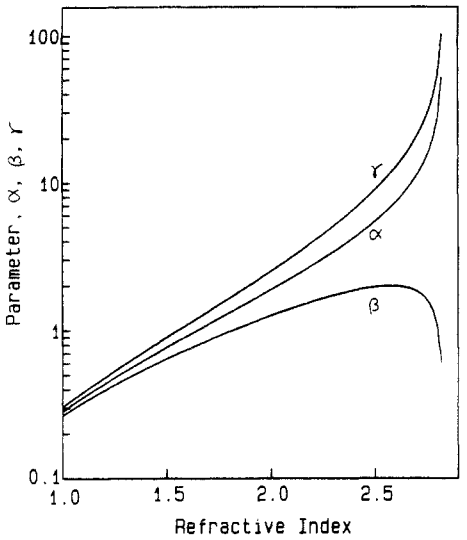

Figure 3. Coefficients α, β, and γ calculated for a germanium crystal ($n_c = 4.0$) and a 45° angle of incidence as functions of the refractive index of the sample sheet.

The constants, A and B, were determined from the requirement for the zero phase shift in the transparent region.

Calculation of the Absorption Index from the ATR Spectrum. The intensities of polarized ATR spectra for the transverse electric wave (TE) and the transverse magnetic wave (TM) can be expressed in terms of three components of absorption index, k_x, k_y, and k_z.[13]

$$\ln R_{TE1} = -\alpha k_x \quad (10)$$

$$\ln R_{TM1} = -\beta k_y - \gamma k_z \quad (11)$$

$$\ln R_{TE2} = -\alpha k_y \quad (12)$$

$$\ln R_{TM2} = -\beta k_x - \gamma k_z \quad (13)$$

where R_{TE1} and R_{TM1} are the reflectivities for the TE and TM waves, respectively, measured with the X axis (extrusion direction) normal to the plane of incidence (Figure 2a), and R_{TE2} and R_{TM2} are obtained with the Y axis (transverse direction) normal to the plane of incidence (Figure 2b). The constants, α, β, and γ, are functions of the angle of incidence and the refractive indices of the sample and the ATR crystal.[13] The values of the coefficients calculated for a germanium crystal ($n_c = 4.0$) and a 45° angle of incidence are shown in Figure 3 as functions of the refractive index of the sample, n_s. If the refractive index, n_s, reaches 2.8, the critical angle approaches the angle of incidence (45°). The values of the coefficients gradually increase with increasing the refractive index of the sample below $n_s = 2.5$.

Results and Discussion

Polarized Specular Reflection Spectrum. Figure 4 shows the specular reflectance of an extrusion molded sheet of the liquid crystalline poly(ester amide). The solid line represents the reflectance measured with polarization parallel to the extrusion direction, and the broken line is the reflectance with perpendicular polarization. The reflectance showed a complicated dispersion in the region of strong absorption. The dichroism in the reflectance reflects the molecular orientation on the surface of the sheet.

The refractive index and the absorption index are shown in Figures 5 and 6, respectively. Baselines of the absorption index dispersion are curved in the wavenumber regions 550–600 cm^{-1} and 1800–1900 cm^{-1}. The curved baselines

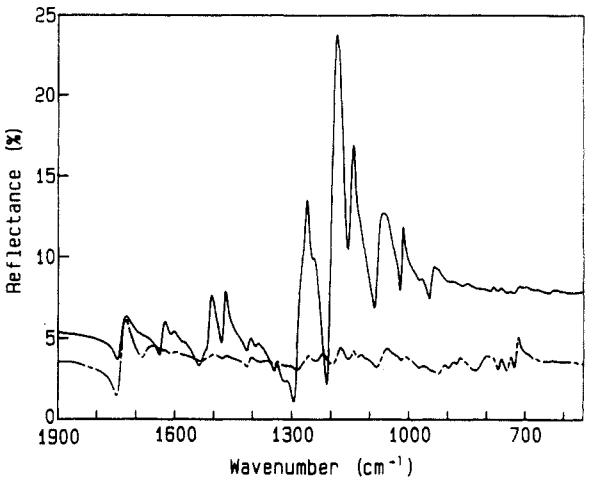

Figure 4. Specular reflectance of a poly(ester amide) sheet (draw-down ratio = 4.07): (—) polarization is parallel to the extrusion direction; (– – –) polarization is perpendicular to the extrusion direction.

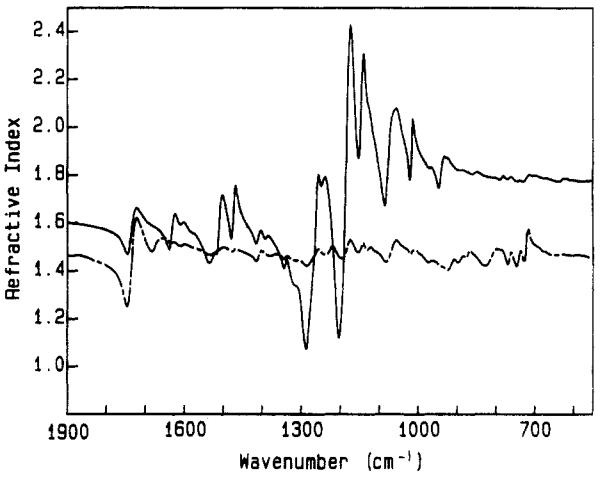

Figure 5. Refractive index of a poly(ester amide) sheet (draw-down ratio = 4.07): (—) polarization is parallel to the extrusion direction; (– – –) polarization is perpendicular to the extrusion direction.

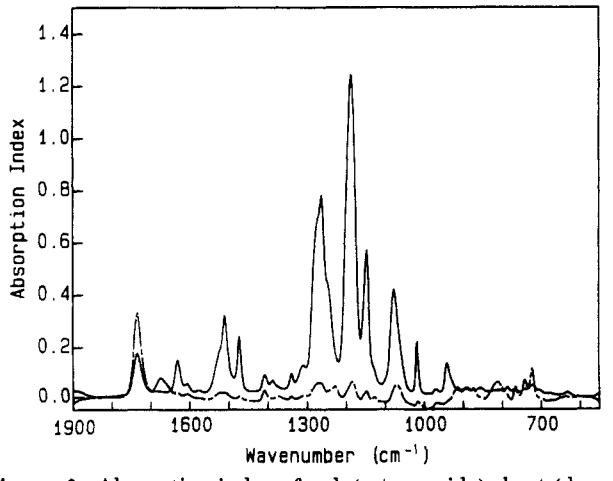

Figure 6. Absorption index of poly(ester amide) sheet (draw-down ratio = 4.07) obtained from specular reflection measurements: (—) polarization is parallel to the extrusion direction; (– – –) polarization is perpendicular to the extrusion direction.

are caused by the limitation of the Roessler equation, in which the reflectance outside the measured region is assumed to be constant.[18,19] The refractive index exhibits a complicated dispersion near strong absorption bands. The refractive index dispersion has a trough on the higher

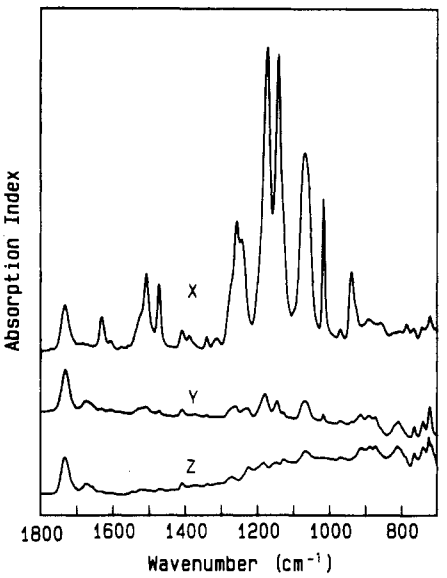

Figure 7. Three components of absorption index of poly(ester amide) sheet (draw-down ratio = 4.07) obtained from polarized ATR spectra.

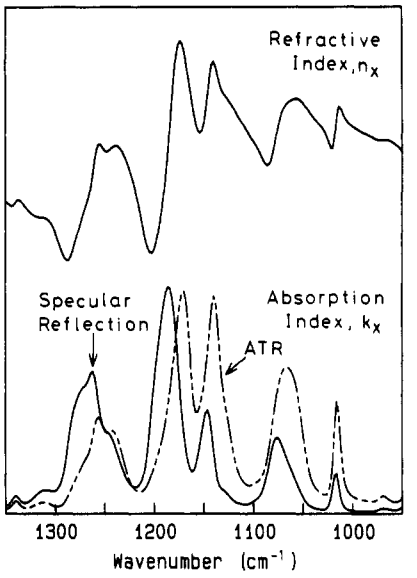

Figure 8. Absorption index, k_x, obtained from ATR (- - -) and specular reflection (—) spectra and the refractive index, n_x.

wavenumber side of the absorption peak and shows a peak on the lower wavenumber side. Some of the absorption bands showed large dichroism, suggesting that the molecular chains were highly oriented at the surface of the sheet. A large birefringence was observed in the wavenumber region 550–1200 cm^{-1}.

One of the limitations of the specular reflection spectroscopy is that the technique is applicable only to films with a smooth surface. The surface of the polymeric material is roughened more or less by the superstructures such as fibrils, liquid crystalline domains, spherulitic structures, etc. The loss of reflectance by surface roughness can be inspected by the observed values of refractive index. The refractive index determined by the specular reflection spectroscopy ranges from 1.4 to 1.8 in the transparent region and lies in the reasonable range of the refractive index of polymer samples.

Polarized ATR Spectrum. Figure 7shows the three components of absorption index dispersion obtained from the polarized ATR spectra. The coefficients α, β, and γ were calculated by assuming that the refractive index of the sample sheet was 1.55 ($\alpha = 0.845, \beta = 0.994, \gamma = 0.696$). A large anisotropy of the absorption index suggests that molecular chains are highly oriented in the surface region of the sheet. The absorption indices, k_y and k_z, exhibits the analogous dispersion forms to each other in the wavenumber region studied. Judging from the agreement of the relative band intensity in k_y with that in k_z, molecular chains in the surface region are uniaxially oriented to the extrusion direction.

The close inspection of the spectra, however, revealed that the absorption intensities in all bands in k_y is slightly higher than those in k_z. A similar problem was addressed by Gupta et al.[10] They measured the polarized ATR spectrum of isotropic polymer sheets and discussed the quantitative accuracy of the intensity ratio for the TE and TM waves in ATR spectroscopy. The theoretical value for $\ln R_{TM}/\ln R_{TE}$, which can be obtained from the coefficients in Figure 3, is 2.0 for the isotropic sheets. They, however, reported that the observed intensity ratio was lower than 2.0. The discrepancy was attributed to the false radiation, resulting from small scratches and chips on the facets.[10] They further reported that the value of $\ln R_{TM}/\ln R_{TE}$ decreased as the sample/crystal contact became looser.[10] We have also measured the polarized ATR spectra of isotropic polymer sheets, such as polypropylene, poly(aryl ether ether ketone), and so on. The observed values of $\ln R_{TM}/\ln R_{TE}$ for the isotropic sheets were 1.4–1.8 in our experiments. As a result, it is difficult to compare the band intensities in the TM wave spectrum quantitatively with the intensities in the TE wave spectrum.

Comparison between the Specular Reflection Spectrum and the ATR Spectrum. Figure 8 shows the X-component of absorption index, k_x, obtained by the ATR and specular reflection techniques, as well as the refractive index dispersion, n_x. In the wavenumber region 1000–1300 cm^{-1}, most of the absorption bands in the ATR spectrum shifted toward the lower wavenumber with respect to the corresponding bands in the specular reflection spectrum. The absorption bands at 1017, 1076, and 1146 cm^{-1} were observed more strongly in the ATR spectrum than in the specular reflection spectrum. The difference might be caused by the large refractive index dispersion in this spectral range. The refractive index abruptly decreases with increasing wavenumber near the absorption maximum. As seen from Figure 3, the constants α, β, and γ increase with increasing the refractive index of the sample. The amplitude of the electric field at the sample/crystal interface depends upon the refractive index and thereby varies with wavenumber in this spectral range. Thus, the refractive index dispersion causes the band distortion and affects the intensity of the ATR spectrum in the spectral region, where intense absorption bands exist.

Figure 9 shows the polarized reflection spectra obtained from the ATR and specular reflection techniques. In the wavenumber region 1350–1800 cm^{-1}, the polarized ATR spectra are in excellent agreement with the absorption index dispersion obtained from the specular reflection technique, except for the intensity of the 1734-cm^{-1} band. The intensity of the 1734-cm^{-1} band in the ATR spectrum, k_y, is lower than that in the specular reflection spectrum, because the refractive index dispersion has a trough near the band peak. The refractive index dispersion does not have serious effects on the ATR spectra in this wavenumber region, where the refractive index is confined in the range 1.3–1.8.

Surface Orientation. If molecular chains orient uniaxially in the extrusion direction, the second moment of

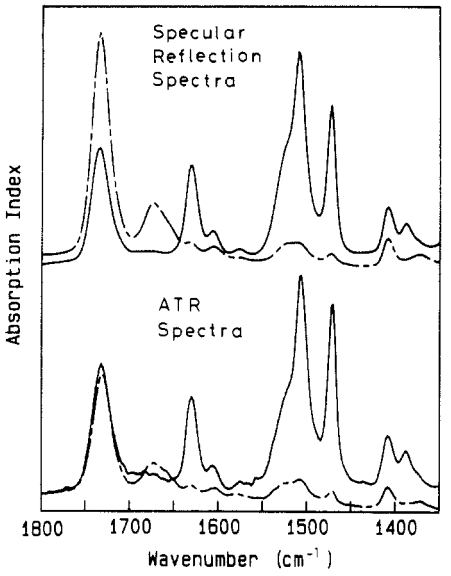

Figure 9. Absorption indices, k_x and k_y, obtained from ATR and specular reflection spectra: (—) polarization is parallel to the extrusion direction; (- - -) polarization is perpendicular to the extrusion direction.

Table I
Orientation Functions Obtained from Polarized Reflection Spectroscopy and Wide-Angle X-ray Diffraction (WAXD)

		orientation functions		
sample	band, cm^{-1}	ATR	specular reflectn	WAXD
sheet A[a]	1632	0.891	0.900	
	1473	0.741	0.778	0.493
	1076	0.760	0.575	
	1017	0.955	0.686	
sheet B[b]	1632	0.940	0.922	
	1473	0.845	0.833	0.763
	1076	0.838	0.536	
	1017	0.952	0.666	

[a] Sheet A: thickness = 0.59 mm, draw-down ratio = 4.07. [b] Sheet B: thickness = 0.19 mm, draw-down ratio = 13.8.

orientation function, f_i, for the i-th absorption band is given by

$$f_i = (D_i - 1)/(D_i + 2) \tag{14}$$

where D_i is the dichroic ratio of the i-th band. Table I shows the orientation functions for two sample sheets with different draw-down ratio. Table I includes values of f_i for four absorption bands, as well as the crystal orientation function, f_c. The absorption bands, which were isolated from the neighboring bands in the spectrum, were used for the analysis.

For 1017- and 1076-cm^{-1} bands, the orientation function obtained from ATR dichroism is higher than that from polarized reflection spectra. The difference is considered to originate from the birefringence effect on the intensity of the ATR spectrum. As seen from Figure 5, the refractive index with parallel polarization is much higher than that with perpendicular polarization in the wavenumber region 1000–1200 cm^{-1}. Therefore, the value of the coefficient, α, for the parallel polarization is much larger than the value for the perpendicular polarization, which leads to the higher estimation of orientation function f_i. On the other hand, for 1632- and 1473-cm^{-1} bands, the orientation function obtained from ATR dichroism is in good agreement with that from the specular reflection spectroscopy. The value of birefringence is small in the wavenumber region above 1350 cm^{-1} (Figure 5).

The orientation function, f_c, obtained from WAXD represents the orientation function of the molecular chain axis in the crystal, while f_i represents the orientation function of the transition moment of the i-th vibrational mode. The orientation function, f, of the molecular chain axis is calculated from f_i, if the angle, ω_i, between the transition moment and the molecular chain axis is known.

$$f = 2f_i/(3\cos^2\omega_i - 1) \tag{15}$$

For the 1632-cm^{-1} band, the observed value of f_i is as high as 0.92–0.94, which provides the lower limit for the orientation function, f, of molecular chains and the higher limit for the transition moment angle, ω_i. The result shows that the orientation function, f, of the sheet is higher than 0.92 and that the transition moment angle for the 1632-cm^{-1} band is smaller than 13°. The transition moment angles of other absorption bands can be estimated from the knowledge of the possible range of molecular orientation function ($0.92 < f < 1.0$). For instance, the transition moment angle for the 1473-cm^{-1} band lies in the range 14.8–19.7°.

In the ATR experiment, the electric field amplitude exponentially decays as a function of depth from the surface:

$$E_z/E_0 = \exp(-\delta Z) \tag{16}$$

where E_0 and E_z are the electric field amplitudes at the surface and at depth Z, respectively. The decay constant, δ, is given by

$$\delta = 2\pi\nu n_c(\sin^2\chi - (n_s/n_c)^2)^{1/2} \tag{17}$$

where χ is the angle of incidence. The value of δ is 2×10^4 cm^{-1} for $\nu = 1500$ cm^{-1}, $\chi = 45°$, $n_c = 4.0$, and $n_s = 1.6$. The ATR spectrum for a 45° angle of incidence and a germanium crystal ($n_c = 4.0$) probes a thin surface layer 0.5 μm thick. The specular reflection spectrum also measures the surface of polymer sheets, because the specular reflection takes place at the surface.

The surface orientation function is higher than the bulk orientation function at lower draw-down ratio (sheet A), while the difference between the surface and bulk orientation functions is smaller at higher draw-down ratio (sheet B). The bulk orientation function increases with increasing draw-down ratio, but the surface orientation function is not so sensitive to draw-down ratio as the bulk orientation function.

The orientation distribution in the sheet is determined by the flow characteristics of the polymer melt. It was reported that the elongational flow was effective for orienting rod-like molecules.[2] The velocity of the polymer flow inside the die was shown to be much lower near the wall than in the central region.[2] After leaving the die, however, the velocity becomes constant along the thickness direction. As a result, fluid elements near the surface are stretched to a higher elongation than those in the central region. Therefore, the degree of orientation at the surface becomes higher than that in the central region. At higher draw-down ratio, fluid elements in the central region are stretched also to an elongation sufficient to form a highly oriented structure. With increasing draw-down ratio, the structure of the polymer sheet becomes uniform along the thickness direction.

Conclusion

The surface orientation of oriented sheets of a liquid crystalline poly(ester amide) was analyzed by the two techniques of reflection infrared spectroscopy: polarized specular reflection and polarized ATR/FTIR. In the region 1350–1800 cm^{-1}, where only weak absorption bands exist,

the polarized ATR spectra are in excellent agreement with the polarized spectra obtained from specular reflection measurements. The reflection infrared spectroscopy was shown to be a reliable method for analysis of the surface structure. For the intense absorption bands, however, one must be careful of the effects of the refractive index dispersion on the ATR spectra, because the large dispersion of refractive index causes the band distortion and modifies the absorption intensity in the ATR spectrum.

The surface orientation function of the liquid crystalline polymer was shown to be higher than the crystal orientation function in the bulk. The bulk orientation function increases with increasing draw-down ratio, but the surface orientation function remains constant. The difference between surface and bulk orientation functions is more marked at lower draw-down ratio. The orientation distribution in the liquid crystalline polymer sheets was discussed in relation to the flow characteristics of the polymer melt.

References and Notes

(1) Shimamura, K.; White, J. L.; Feller, J. F. *J. Appl. Polym. Sci.* **1981**, *26*, 2165.
(2) Ide, Y.; Ophir, Z. *Polym. Eng. Sci.* **1983**, *23*, 261.
(3) Chung, T.-S. *J. Polym. Sci., Polym. Lett. Ed.* **1986**, *24*, 299.
(4) Takeuchi, Y.; Shuto, Y.; Yamamoto, F. *Polymer* **1988**, *29*, 605.
(5) Weng, T.; Hiltner, A.; Baer, E. *J. Mater. Sci.* **1986**, *21*, 744.
(6) Sung, C. S. P. *Macromolecules* **1981**, *14*, 591.
(7) Hobbs, J. P.; Sung, C. S. P.; Krishnan, K.; Hill, S. *Macromolecules* **1983**, *16*, 193.
(8) Mirabella, F. M., Jr. *J. Polym. Sci., Polym. Phys. Ed.* **1984**, *22*, 1283.
(9) Mirabella, F. M., Jr. *J. Polym. Sci., Polym. Phys. Ed.* **1984**, *22*, 1293.
(10) Gupta, M. K.; Carlson, D. J.; Wiles, D. M. *J. Polym. Sci., Polym. Phys. Ed.* **1984**, *22*, 1011.
(11) Pirnia, A.; Sung, C. S. P. *Macromolecules* **1988**, *21*, 2699.
(12) Zerbi, G.; Gallino, G.; Del Fanti, N.; Baini, L. *Polymer* **1989**, *30*, 2324.
(13) Flournoy, P. A.; Schaffers, W. J. *Spectrochim. Acta* **1966**, *22*, 5.
(14) Jahoda, F. C. *Phys. Rev.* **1957**, *107*, 1261.
(15) Kato, R. *J. Phys. Soc. Jpn.* **1961**, *16*, 2525.
(16) Phillip, H. R.; Ehrenreich, H. *Phys. Rev.* **1963**, *131*, 2016.
(17) Phillip, H. R.; Taft, E. A. *Phys. Rev.* **1964**, *136*, 1445.
(18) Roessler, D. M. *Br. J. Appl. Phys.* **1965**, *16*, 1119.
(19) Roessler, D. M. *Br. J. Appl. Phys.* **1966**, *17*, 1313.
(20) Desjardins, S. R.; Wilcox, D. E.; Musselman, R. L.; Solomon, E. I. *Inorg. Chem.* **1987**, *26*, 288.
(21) Musselman, R. L. *Microbeam Anal.* **1989**, *24*, 151.
(22) Robinson, T. S.; Price, W. C. *Proc. Phys. Soc., Ser. B* **1953**, *66*, 969.
(23) Nakagawa, I. *Bull. Chem. Soc. Jpn.* **1971**, *44*, 3014.
(24) Nakagawa, I. *Spectrochim. Acta* **1973**, *29A*, 1451.
(25) Kaito, A.; Nakayama, K.; Kanetsuna, H. *J. Polym. Sci., Polym. Phys. Ed.* **1988**, *26*, 1439.
(26) Kaito, A.; Nakayama, K.; Kyotani, M. *J. Polym. Sci., Polym. Phys. Ed.* **1991**, *29*, 1321.

Registry No. (2-Hydroxy-6-naphthoic acid)(4-aminophenol)-(terephthalic acid) (copolymer), 98209-52-0.